Analytical Method for Predicting the Air-Gap Flux of Interior-Type Permanent-Magnet Machines

Chunting Mi, *Senior Member, IEEE*, Mariano Filippa, *Student Member, IEEE*, Weiguo Liu, and Ruiqing Ma

***Abstract*—This paper presents an analytical method to calculate the air-gap magnetic flux of interior-type permanent-magnet (IPM) machines taking into account the assembly gap and saturation in stator and rotor. Special considerations are given to the calculation of leakage flux in the nonlinear magnetic short circuit or the "magnetic bridges." An equivalent magnetic circuit was developed, and a computer-aided graphic analysis program calculated the magnet operating point. The Norton equivalent of flux concentration structures was studied. Agreements have been obtained between the results of the analytical model, finite-element analysis, and test results on prototype motors.**

***Index Terms*—Computer-aided design (CAD), finite-element analysis (FEA), graphic theory, magnetic circuits, permanent-magnet machines, permanent-magnet motors, permanent magnets.**

I. Introduction

INTERIOR-TYPE permanent-magnet (IPM) motors are used in a wide range of industrial applications due to their robustness, simplicity, and ease of flux weakening control [1]–[7]. When permanent magnets (PMs) are buried inside the rotor laminations, magnets are inserted into the prepunched slots and need not be glued such as in surface mounted magnets motors [3]. In IPM motors, magnets are protected from flying away from the rotor surface due to centrifugal force, fatigue, and aging of material during operation of the motor. Rectangular (cuboid) magnets can be used in IPM motors to simplify the manufacturing process and reduce the cost of manufacturing PM material. Flux concentration structures are often used to increase air-gap flux density in IPM motors.

Air-gap flux is one of the most important parameters of PM motor designs. Calculating air-gap flux in IPM motors is somewhat troublesome due to the existence of so-called "magnetic bridges." When an integrated lamination is used for IPM motors, magnetic short circuits exist around the edges of the magnets. These magnetic bridges are designed to provide integrity to the rotor. These magnetic bridges introduce magnetic short circuits and complicate the design and analysis of IPM motors. On the other hand, there are also concerns on how to limit the leakage flux in these magnetic bridges while maintaining the mechanical strength of the rotor. The flux leakage and flux distribution in these magnetic bridges can be precisely obtained through numerical methods such as finite-element analysis (FEA). However, FEA can only be performed after the preliminary dimensions of the motor have been determined. FEA is also cumbersome and time consuming in the early stages of PM motor design where numerous iterations are usually performed. Analytical calculation and analysis of all types of PM motors are essential in their early design stage [8], [9].

Rahman and Slemon [9] proposed an analytical model for an IPM motor. The leakage flux was not specifically dealt with. Hwang and Cho [10] and Tsai and Chang [11] performed similar studies on the influence of flux leakage in IPM motors using an equivalent magnetic circuit method. In their research, flux density in the magnetic bridges was assumed to be constant. Saturation and the reluctance of the iron were neglected. Lovelace *et al.* developed a saturating lumped-parameter model for an IPM synchronous machine [12]. Emphasis was placed on using equivalent magnetic circuits to determine the parameters of IPM motors. In almost all previous studies, the assembly gap between magnet and laminations was neglected.

This paper presents an analytical method to calculate the air-gap flux of IPM machines using an equivalent magnetic circuit model taking into account the assembly gap and saturation in the steel. Graphic analysis and computer-aided design (CAD) analysis were employed to solve the magnetic operating point. Verified by numerical methods and experiments, the proposed method provides machine designers a simple yet accurate approach to design IPM motors. The paper further discusses factors that affect the flux leakage in an IPM motor and the influence of the sizes of magnetic bridges.

II. Flux Distribution in IPM Motors

Fig. 1 shows four commonly used IPM rotor configurations. Fig. 1(a) and (b) use circumferential-type magnets. Fig. 1(b) is mainly used for line-start synchronous motor. Configurations of Fig. 1(a) and (b) are usually used for motors with six or more poles. Fig. 1(c) uses inserted magnets. Fig. 1(d) uses inset magnets.

Fig. 2 shows the configuration and no-load flux distribution of an eight-pole circumferential-type IPM line-start synchronous motor calculated using FEA. Integrated laminations are used to keep the integrity of the rotor. It contains three magnetic bridges in each pole: Bridge I between the magnet and rotor slot, and Bridge II and III at the interpolar space between the magnet and the shaft. Fig. 3 shows the flux density along Line I of Fig. 2. It can be seen from Fig. 3 that the flux densities differ in the two bridges.

Manuscript received June 8, 2003; revised September 17, 2003. This work was supported by the University of Michigan, Dearborn, under the CEEP Grant.

C. Mi and M. Filippa are with the Department of Electrical and Computer Engineering, University of Michigan, Dearborn, MI 48128 USA (e-mail: chrismi@umich.edu).

W. Liu and R. Ma are with the Department of Automation, Northwestern Polytechnic University, Xi'an 710072, China (e-mail: lwglll@nwpu.edu.cn).

Digital Object Identifier 10.1109/TMAG.2003.821562

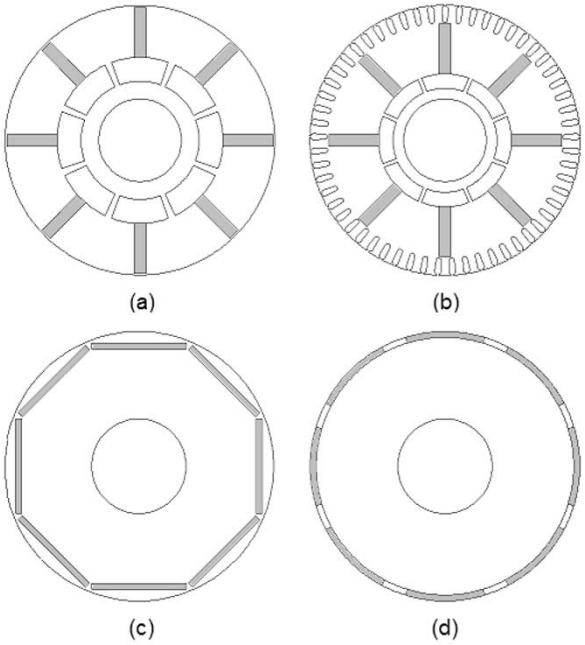

Fig. 1. Four commonly used IPM rotor configurations: (a) circumferential-type magnets suitable for brushless dc or synchronous motor, (b) circumferential-type magnets suitable for line-start synchronous motor, (c) inserted magnets, and (d) inset magnets.

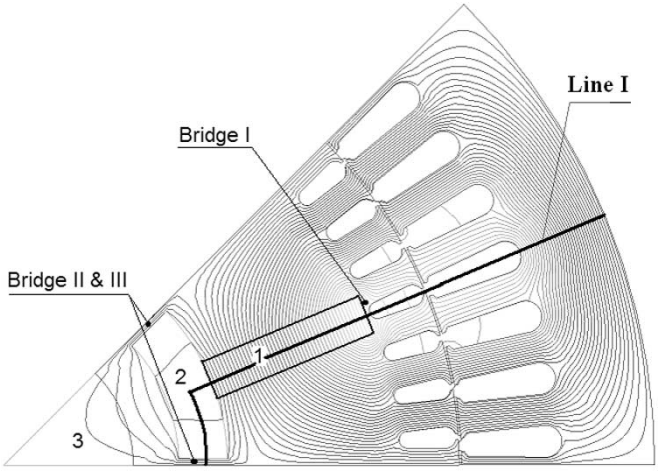

Fig. 2. Flux distribution of an IPM line-start synchronous motor with circumferential-type magnets. 1: Magnet. 2: Nonmagnetic material. 3: Shaft.

It will be shown later that the magnetic flux density in the magnetic bridges is related to the width and length of the magnetic bridge, rather than constant as assumed in [10] and [11]. In the meantime, there is flux leakage in the rotor slot and the nonmagnetic material between the magnet and the shaft. The flux leakage through the stator slot is negligible.

III. Norton Equivalent of Magnets

Modern rare-earth permanent magnets (REPMs) have a straight demagnetization curve, as shown in Fig. 4. The low cost makes Nd–Fe–B REPMs ideal for motor applications. However, temperature effects, as shown in Fig. 4, must be taken into consideration when designing a PM motor.

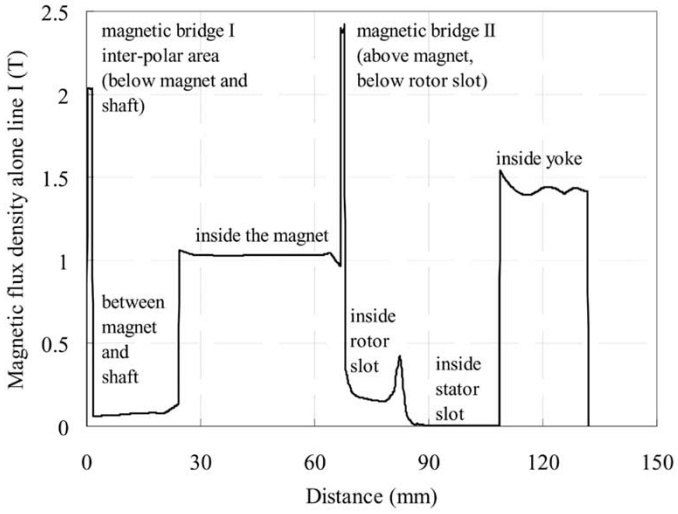

Fig. 3. Flux density along Line I of Fig. 1.

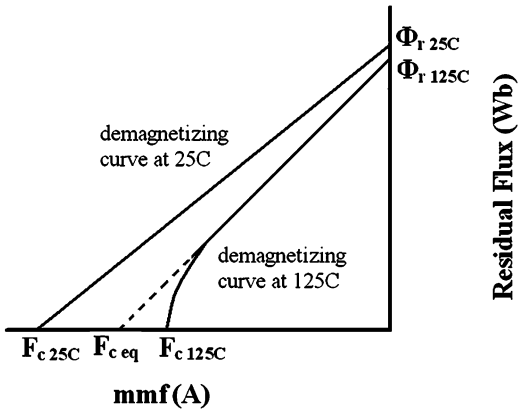

Fig. 4. Demagnetization curve of Nd–Fe–B magnets considering temperature effects, where subscript 25 °C represents its value at room temperature, whereas subscript 125 °C represents its value at 125 °C. F_{ceq} is the equivalent MMF of the linear portion of the demagnetizing curve.

Under room temperature (25 °C), the demagnetizing curve of a cuboid REPM can be represented by

$$\Phi_m = \Phi_r - F_m \cdot \frac{\Phi_r}{F_c} = \Phi_r - \frac{F_m}{R_M} \tag{1}$$

where Φ_r and F_c are residual flux and magnetomotive force (MMF) of each pole, respectively, and R_M is the reluctance of the magnet, which is the reverse of magnet permeance λ_M

$$R_M = \frac{1}{\lambda_M} = \frac{F_c}{\Phi_r}. \tag{2}$$

For parallel or circumferentially magnetized poles as shown in Fig. 1(a) and (b)

$$\Phi_r = 2B_r A_m, \quad F_c = l_m H_c. \tag{3}$$

While for series or radially magnetized poles as shown in Fig. 1(c) and (d)

$$\Phi_r = B_r A_m, \quad F_c = 2l_m H_c \tag{4}$$

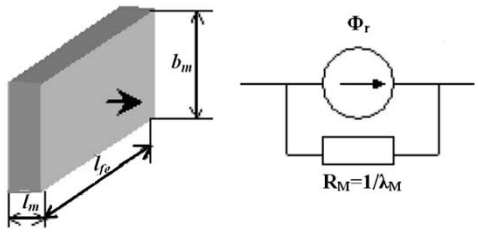

Fig. 5. Norton equivalent of cuboid magnets.

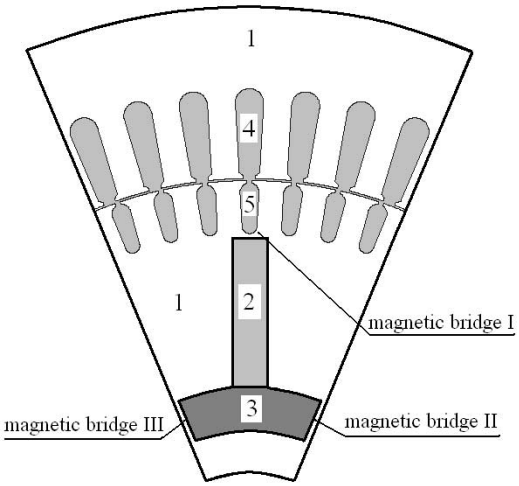

Fig. 6. Arrangements of magnets of line-start IPM motors. 1: Stator and rotor iron laminations. 2: Permanent magnets. 3: Nonmagnetic material. 4: Stator slots. 5: Rotor slots. Magnetic bridges are part of the rotor laminations to keep the integrity of rotor laminations. Fluxes passing through these bridges are leakage fluxes. These magnetic bridges are highly saturated, as can be seen from Fig. 2.

where B_r and H_c are remanence and coercive force of the magnets, respectively, l_m is the length of the magnet, and A_m is the cross-sectional area

$$A_m = b_m l_{fe} \tag{5}$$

where l_{fe} is the length of magnet along the shaft direction and usually equal to the rotor lamination stack length.

At operating temperature, the above parameters are replaced by their respective values at the operating temperature. It is possible that the demagnetizing curve becomes nonlinear at operating temperature. In this case, F_{ceq} should be used in place of F_c, as shown in Fig. 4. The Norton equivalent of a cuboid magnet is shown in Fig. 5.

IV. No-Load Equivalent Magnetic Circuit Analysis of IPM Machines

A typical circumferentially magnetized IPM rotor configuration is shown in Fig. 6. The equivalent magnetic circuit of this configuration is shown in Fig. 7(a), where R_δ, R_{y1}, R_{y2}, R_{t1}, R_{t2}, R_σ, R_1, R_2, and R_S are the reluctances of air gap, stator yoke, rotor yoke, stator teeth, rotor teeth, assembly gap between magnets and laminations, magnetic bridge I, magnetic bridge II and III (combined due to symmetry), and leakage through rotor slots and the nonmagnetic material, respectively. End effects are neglected.

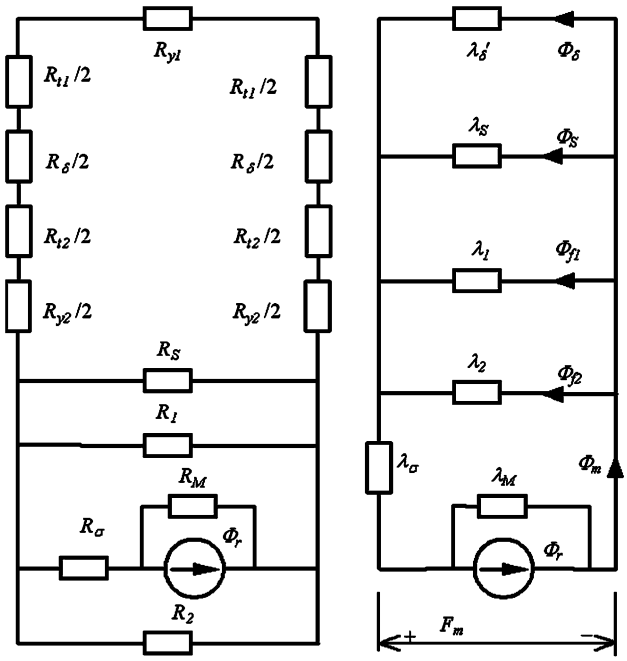

Fig. 7. Equivalent magnetic circuit of IPM motors with circumferential magnets. (a) Exact model. (b) Simplified model.

The magnetic circuit can be simplified, as shown in Fig. 7(b), where λ'_δ is the total permeance combining air gap, stator teeth, stator yoke, rotor teeth (if any), and rotor yoke; λ_1 is the permeance of magnetic bridge I; λ_2 is the permeance of magnetic bridges II and III; and λ_S is the total permeance leakage through rotor slot and nonmagnetic material. Let

$$\begin{aligned} \lambda'_\delta &= \frac{1}{(R_\delta + R_{t1} + R_{t2} + R_{y1} + R_{y2})} \\ \lambda_o &= \lambda'_\delta + \lambda_1 + \lambda_2 + \lambda_S \\ \lambda_{\text{ex}} &= \lambda_o \parallel \lambda_\sigma \end{aligned} \tag{6}$$

where λ_{ex} is the total external permeance.

Solving the magnetic circuit, the magnet operating point and all fluxes can be found

$$\begin{aligned} F_m &= \frac{\Phi_r}{(\lambda_M + \lambda_{\text{ex}})} \\ \Phi_m &= \frac{\Phi_r \lambda_{\text{ex}}}{(\lambda_M + \lambda_{\text{ex}})} \end{aligned} \tag{7}$$

$$\sum F = F_m - \frac{\Phi_m}{\lambda_\sigma}$$

$$\Phi_\delta = \lambda'_\delta \sum F$$

$$\Phi_f = (\lambda_1 + \lambda_2) \sum F$$

$$\Phi_S = \lambda_S \sum F \tag{8}$$

$$\Phi_m = \Phi_\delta + \Phi_f + \Phi_S \tag{9}$$

where Φ_δ is the total air-gap flux, Φ_f is the total leakage flux in the magnetic bridges, and Φ_s is the total leakage flux in rotor slot and the nonmagnetic material.

It can be seen from Figs. 6 and 7 that the magnetic bridges shall have the same MMF as that of the air-gap branch. Therefore, magnetic field density of each of the bridges is

$$H_f = \frac{\sum F}{l_f} \tag{10}$$

where l_f is the length of the magnetic bridge along the flux path. It can be seen from (10) that if the magnetic bridges have different path for magnetic fluxes, then the field density will be different.

The flux density in each of the bridges can be found through table lookup or curve-fitting of the lamination material. Total flux leakage in each of the magnetic bridges can be expressed as

$$\Phi_f = B_f A_f \tag{11}$$

where B_f is the flux density in the magnetic bridges, and A_f is the cross-sectional area of that magnetic bridge.

V. Magnet Operating Point

Although (7)–(9) give an analytical expression for air-gap flux, it can hardly be solved due to saturation in the yoke, teeth, and the magnetic bridges. Graphic analysis is an effective method to solve the operating point of the magnets.

A. Unsaturated Motor

If the yoke and teeth of the motor are not saturated but the magnetic bridges are highly saturated, further, if the assembly air gap is neglected, the air-gap flux can be calculated analytically.

Assume that the flux density in the magnetic bridges is constant due to high saturation. Then

$$\Phi_\delta = \frac{\lambda_\delta}{\lambda_\delta + \lambda_M + \lambda_S}(\Phi_r - \Phi_f) \tag{12}$$

where air-gap permeance can be expressed as

$$\lambda_\delta = \frac{\alpha \tau l_{fe} \mu_0}{2\delta k_\delta} \tag{13}$$

where α is the effective pole-width coefficient, τ is the pole pitch, k_δ is Carter's coefficient, δ is air-gap length, and μ_0 is the permeability of air $\mu_0 = 4\pi \times 10^{-7}$ T · m/A.

Carter's coefficient can be calculated for stator slots and rotor slots (if any) separately [2], [13], [14], e.g.,

$$k_\delta = k_{\delta 1} k_{\delta 2} \tag{14}$$

$$k_{\delta 1} \text{ or } k_{\delta 2} = \frac{t}{(t - \gamma^* \delta)} \tag{15}$$

$$\gamma = \frac{4}{\pi}\left[\frac{b_0}{2\delta}\tan^{-1}\left(\frac{b_0}{2\delta}\right) - \ln\sqrt{1+\left(\frac{b_0}{2\delta}\right)^2}\right] \tag{16}$$

where b_0 is the width of the slot opening, and t is the slot pitch.

Leakage permeance λ_S can also be found for rotor slots and the nonmagnetic material by using equations given in [2], [13], and [14]. Reluctance of assembly air gap can be expressed as a function of σ, where σ is the average tolerance between the magnet and the lamination steels. The reluctance of the assembly air gap is

$$\lambda_\sigma = \frac{b_m l_{fe} \mu_0}{\sigma}. \tag{17}$$

TABLE I
Magnetic Circuit Calculation of Experimental Motor

1	B_δ	(Experimental motor)	0.8	0.9
2	$B_t = t/b_t B_\delta$	$B_t = 2.02B_\delta$	1.6	1.8
3	H_t (*Look−up−Table*)	H_t	4250.0	13280.0
4	$F_t = h_t H_t$	$F_t = 0.04H_t$	181.1	565.7
5	$B_y = \Phi_\delta / 2h_y l_{fe}$	$B_y = 1.38B_\delta$	1.1	1.2
6	H_y (*Look−up−Table*)	H_y	498.6	742.8
7	$F_y = l_y H_y$	$F_y = 0.12H_y$	59.3	88.4
8	$F_\delta = 1.6\delta k_\delta B/\mu_0$	$F_\delta = 566.8B_\delta$	907.1	1020.5
9	$\sum F = F_\delta + F_t + F_y$	$\sum F = F_\delta + F_t + F_y$	1147.5	1674.6
10	$H_{f1} = \sum F / l_{f1}$	$H_{f1} = \sum F / l_{f1}$	229498.0	334923.3
11	B_{f1} (*Look−up−Table*)	B_{f1}	2.29	2.43
12	$H_{f2} = \sum F / l_{f2}$	$H_{f2} = \sum F / l_{f2}$	95624.2	139551.4
13	B_{f2} (*Look−up−Table*)	B_{f2}	2.12	2.17
14	$\Phi_\delta = \alpha\tau l_{fe} B_\delta$	$\Phi_\delta = 14.08\times10^{-3} B_\delta$	0.011263	0.012671
15	$\Phi_{f1} = B_{f1} A_{f1}$	$\Phi_{f1} = 0.38\times10^{-3} B_{f1}$	0.001743	0.001848
16	$\Phi_{f2} = B_{f2} A_{f2}$	$\Phi_{f2} = 0.608\times10^{-3} B_{f2}$	0.001287	0.001322
17	$\Phi_s = \sum F \lambda_S$	$\Phi_s = 0.336\times10^{-6} F_m'$	0.000771	0.001125
18	$\Phi_m = \Phi_\delta + \Phi_{f1} + \Phi_{f2} + \Phi_s$	Φ_m	0.015063	0.016966
19	$F_m = \sum F + \Phi_m / \lambda_\sigma$	F_m	1462.9	2029.9

b_{t1} and h_{t1} are the width and height of stator slots; b_{t2} and h_{t2} are the width and height of rotor slots; l_{y1} and h_{y1} are the length and height of stator yoke; l_{y2} and h_{y2} are the length and height of rotor yoke; A_{f1} and A_{f1} are the cross-sectional area of each magnetic bridge; l_{f1} and l_{f2} are the length of each magnetic bridge, respectively.

B. Tabulation and Graphic Analysis

When the IPM motor is saturated as is the case for most PM motor designs, graphic analysis can be used to solve the magnetic operating point. Detailed steps of graphic analysis are shown in Table I and Fig. 8. The calculation procedure is detailed in the following.

1) Assume an air-gap flux density B_δ, as shown in Table I, row 1.
2) Calculate the flux density in the stator tooth (row 2); use table lookup or curve fitting to find the magnetic field density H_t in the tooth (row 3); calculate the MMF of the tooth (row 4).
3) Repeat step 2) to calculate the MMF of the rotor tooth, stator yoke, and rotor yoke (rows 5 to 7).
4) Calculate the air-gap MMF (row 8).
5) Calculate the subtotal MMF by summing air-gap MMF and core MMF (row 9).
6) Calculate the magnetic field density of the magnetic bridges (rows 10 and 12); Use lookup table or curve fitting to find the magnetic flux density B_f in the magnetic bridges (rows 11 and 13).

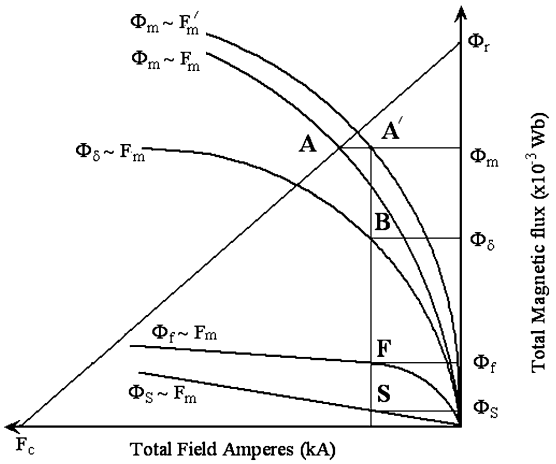

Fig. 8. Graphic analysis of no-load IPM machine, where cross point A is the operating point of magnet, B represents the air-gap flux, F represents the leakage flux in the magnetic bridges, and S represents the leakage flux in rotor slots and the nonmagnetic material. Note that the leakage flux in the magnetic bridges contributes a significant portion of the total flux supplied by magnet, as can be seen on the graph.

7) Calculate the air-gap flux, leakage flux in the bridges, and leakage flux through the rotor slots (rows 14 to 17).
8) Calculate the total flux (row 18) and total MMF (row 19).
9) Plot five curves in the second quadrant as shown in Fig. 8 using Table I. Find on the graph the cross point A. This is the magnet operating point. Plot a horizontal line to cross with $\Phi_m \sim F_m$ at A'. Plot a vertical line down from Point A'. The cross point of this vertical line with curve $\Phi_\delta \sim F_m$ is air-gap flux, where $\Phi_S \sim F_m$ is leakage flux through rotor slot, and $\Phi_f \sim F_m$ is leakage flux through the bridges.

C. Graphic Analysis of Loaded Motor

The operating point of magnets at rated load can also be solved by shifting the air-gap curve $\phi_\delta \sim F_m$ by F_{ad} to the left on the graph, where F_{ad} is the armature MMF.

VI. Computer-Aided Design and Analysis

Although the above graphic analysis is perceivable, it involves massive calculation and may not be accurate. CAD is an essential tool to solve the magnetic operating point.

The definition of the problem is to find the solution between linear function (1) and nonlinear function $\Phi_m = f(F_m)$, which is tabulated in Table I; or alternatively, find the cross point A on Fig. 8. It becomes a one-dimensional optimization problem

$$\min f_1(F_m) \tag{18}$$

where

$$f_1(F_m) = \Phi_r - F_m\lambda_M - f(F_m). \tag{19}$$

When (19) is minimized, the solution for F_m is found. A linear search algorithm can be used. The flowchart of the algorithm is shown in Fig. 9. A CAD program was developed using Microsoft Excel with its embedded Visual Basic Macros to design the IPM motor as well as solve for the magnetic operating point. The interface of the CAD program is shown in Fig. 10.

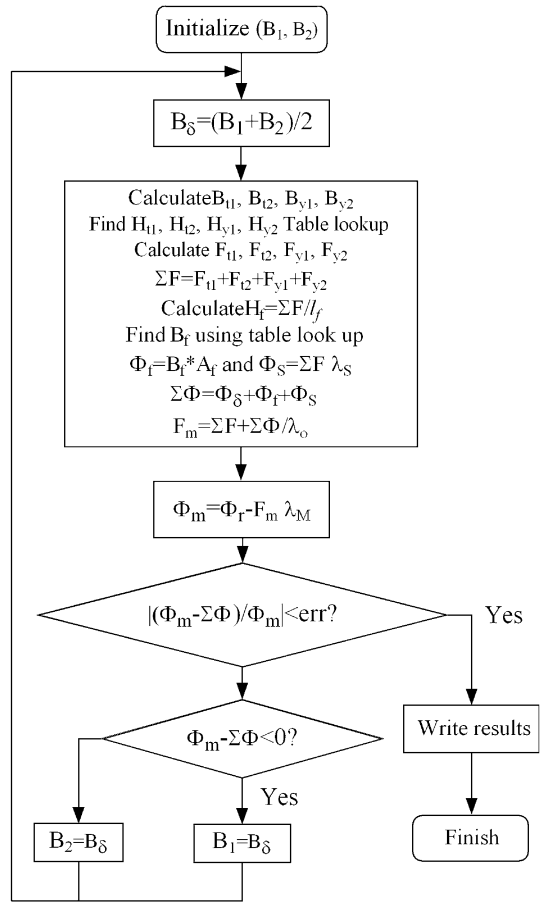

Fig. 9. Flowchart used for solving the magnet operating point.

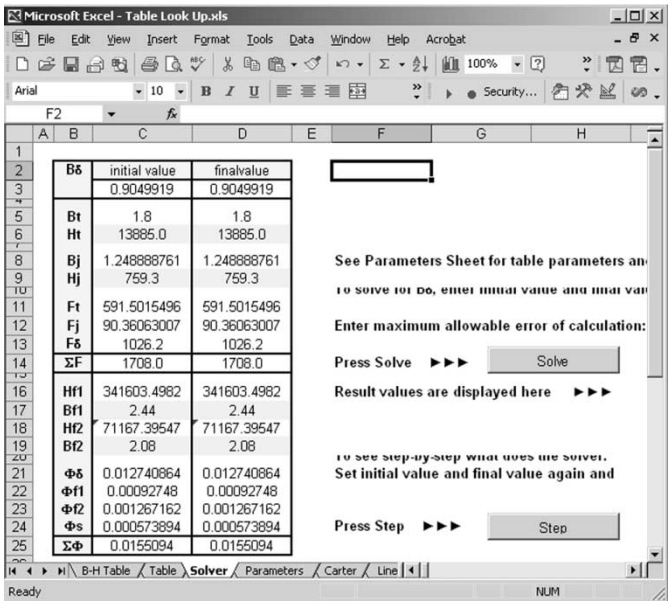

Fig. 10. CAD program to design and solve the magnetic operating point of IPM machines using an analytical method.

The overall calculation time hardly exceeds a few minutes for a complete IPM motor design.

The CAD program can be used for the initial design of IPM motors to save design time. By entering motor ratings to the

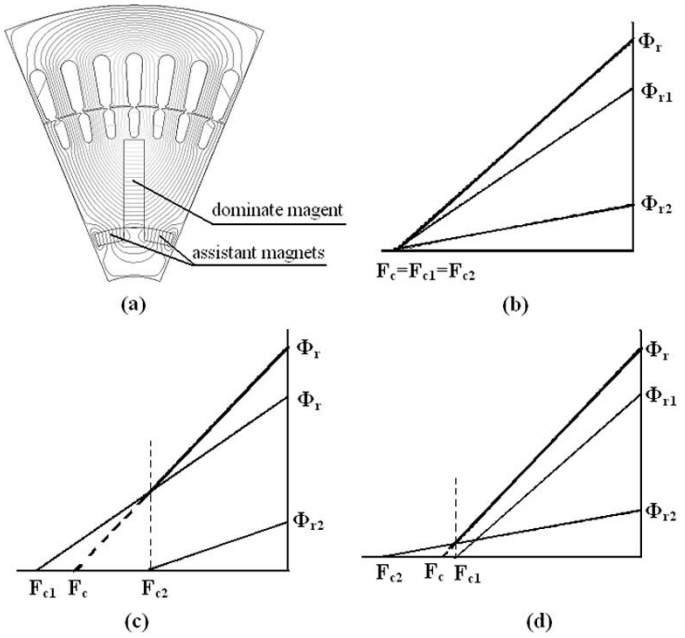

Fig. 11. Flux concentration configurations. (a) Configuration with the assistant magnets in series. (b) Equivalent demagnetizing curve when the assistant magnets have the same MMF as that of the dominant magnet. (c) When MMF of assistant magnets is more than that of the dominant magnet. (d) When MMF of assistant magnets is less than that of the dominant magnet.

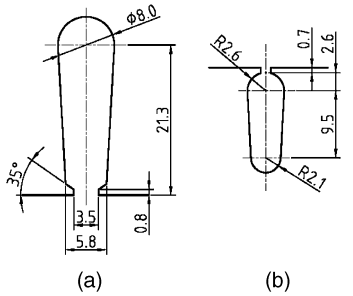

Fig. 12. Rotor and stator slot dimensions of the first experimental motor. (a) Stator slot dimensions—54 slots. (b) Rotor slot dimensions—58 slots.

spreadsheet, the program calculates the initial dimensions of the motor. The magnet operating point is instantaneously solved. The program can also generate initial drawings for FEA uses. By setting the width of magnetic bridges to zero, the CAD program is also capable of design surface-mounted and inset-magnet PM motors.

VII. Norton Equivalent of Magnets in Flux Concentrate Configurations

Flux concentration configurations are often used in IPM machines to increase air-gap flux density, as shown in Fig. 11(a). In flux concentration configurations, the assistant magnets are usually designed to have the same MMF as the dominant magnet. However, due to dimension and other constraints, the assistant magnets may have a different MMF.

There are three possibilities, as shown in Fig. 11(b)–(d). The Norton equivalent of all magnets can still be expressed by (1), with Φ_r and F_c the equivalent residual flux and equivalent MMF, and R_M the equivalent reluctance. The equivalent Φ_r and F_c can be expressed as

$$\Phi_r = \Phi_{r1} + \Phi_{r2} \tag{20}$$

$$F_c = \frac{\Phi_r}{\Phi_{r1}F_{c2} + \Phi_{r2}F_{c1}} F_{c1}F_{c2} \tag{21}$$

where Φ_{r1} and F_{c1} are the residual flux and MMF of the dominant magnet, and Φ_{r2} and F_{c2} are the residual flux and MMF of the assistant magnet.

TABLE II
Dimensions and Parameters of the Experimental Motor

Name	Value	Name	Value
Inner radius of stator (mm)	230	Width of magnets (mm)	32
Outer radius of stator (mm))	327	Airgap length (mm)	0.6
Thickness of magnets (mm)	9.8	Stack length (mm)	190
Stator number of slots	54	Rotor number of slots	58
Stator turns per phase	171	Winding factor	0.9489

TABLE III
Comparison of Fluxes Between Predicted and FEA Neglecting Saturation and Assuming Constant Flux Density in Magnetic Bridges

	Predicted	FEA	Error (%)
Airgap flux (Wb)	0.01243	0.01113	11.6
Magnet Flux (Wb)	0.01586	0.01584	0.1
Flux leakage in magnet bridge (Wb)	$2.74\text{x}10^{-3}$	$1.733\text{x}10^{-3}$	58.0
Flux leakage in rotor slot (Wb)	$0.67\text{x}10^{-3}$	$1.280\text{x}10^{-3}$	47.6

VIII. Numerical and Experimental Verification

In order to verify the proposed analytical method, numerical analysis and experiments were performed on two IPM motors. The first experimental motor is a 15 kW, eight-pole, 380 V (delta connected), 50 Hz, 750 r/min, circumferentially organized IPM motor. Motor dimensions and parameters are shown in Table II. Rotor and stator slot dimensions are shown in Fig. 12. Magnets are Nd–Fe–B N35SH with $B_r = 1.21$ T, $H_c = 883.5$ kA/m, and $H_{cJ} = 1600$ kA/m, with dimension 190 mm $\times$ 40 mm $\times$ 9.8 mm. The assembly air gap is 0.2 mm.

Carter's coefficient are calculated for the stator slots and rotor slots, respectively, being $k_{\delta 1} = 1.136$, $k_{\delta 2} = 1.045$ and $k_\delta = k_{\delta 1} * k_{\delta 2} = 1.187$ Wb/A. The leakage permeance through rotor slots and the nonmagnetic material are found to be $\lambda_S = 0.336 \times 10^{-6}$.

The air-gap flux was calculated neglecting saturation and assuming a constant flux density in the bridges. The results are compared with those obtained by FEA in Table III, with discrepancy being 11% between predicted and FEA results.

The magnetic flux of the motor was then calculated using the analytical method taking into account saturation. The calculated fluxes by the proposed method are compared with those calculated by FEA in Table IV. It can be seen from Table IV that the predicted fluxes and flux densities in different areas of the motor agree with those obtained by FEA, with discrepancies generally less than 3%. This validates the proposed analytical method.

TABLE IV
COMPARISON OF FLUXES BETWEEN PREDICTED, FEA METHOD AND MEASUREMENT TAKING INTO ACCOUNT SATURATION

	Predicted	FEA	Error (%)
Airgap flux (Wb)	0.01125	0.01113	1.1
Magnet Flux (Wb)	0.01505	0.01584	5.3
Flux leakage in bridge (Wb)	0.00303	0.00301	0.7
Flux density in bridge I (T)	2.29	2.280	0.4
Flux density in bridge II (T)	2.12	2.106	0.7
Flux leakage in slot (Wb)	$0.76\text{x}10^{-3}$	$0.78\text{x}10^{-3}$	2.6

TABLE V
COMPARISON OF EMF BETWEEN PREDICTED AND EXPERIMENTS OF THE FIRST EXPERIMENTAL MOTOR (VOLTS)

Speed (rpm)	Proposed method	Measurement	Error (%)
350	189	185	2.22
588	318	308	3.15
650	351	345	1.80
715	386	372	3.85
750	405	395	2.59
770	416	405	2.73

The back EMF of the motor can be calculated for each speed using

$$E_o = 4.44 f W k_w \Phi_\delta \tag{22}$$

where f is frequency, W is number of turns per phase, and k_w is winding factor.

The EMF of the experimental motor was then measured and compared to those calculated in Table V. Table V shows the difference between the predicted and measured air-gap flux is below 3%.

A second verification was performed on an IPM motor with radially arranged magnets. The motor is rated at 22 kW, six-pole, 380 V, 50 Hz. The motor and magnet arrangement are shown in Fig. 13 with its flux distributions.

This motor uses the same stator laminations and stack length as in the first motor. Air-gap length is 0.8 mm. Magnets are also Nd–Fe–B N35SH with sizes of 100 mm $\times$ 220 mm $\times$ 6 mm each pole. Stator turns per phase is 124. Table VI shows the comparison between the predicted and measured fluxes. Again, the discrepancy between predicted and measured is below 7%.

To further verify the proposed method, an asymmetrically arranged IPM motor is analyzed as shown in Fig. 14. The air-gap flux was calculated using both the proposed method and FEA. It is shown that the discrepancy between the two methods is only 3.4%.

IX. DISCUSSION OF LEAKAGE OF MAGNETIC FLUX IN MAGNETIC BRIDGES

The flux leakage coefficient σ_o is defined as $\sigma_o = \Phi_m/\Phi_\delta$, which reflects the usage of the magnet flux. Neglecting the assembly air gap, the leakage coefficient can be expressed as

$$\sigma_o = \frac{(\Phi_\delta + \Phi_f + \Phi_S)}{\Phi_\delta} = \frac{(\lambda'_\delta + \lambda_1 + \lambda_2 + \lambda_S)}{\lambda'_\delta}. \tag{23}$$

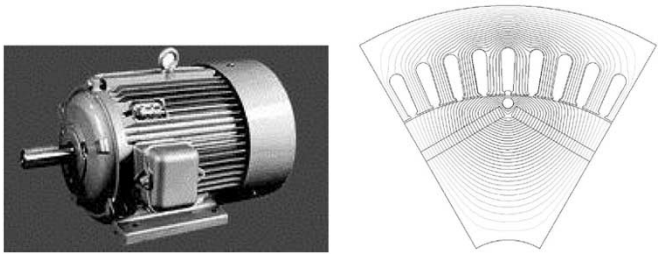

Fig. 13. Flux distribution of a radial-type 22 kW, eight-pole brushless IPM motor.

TABLE VI
COMPARISON OF FLUXES BETWEEN PREDICTED, FEA METHOD, AND MEASUREMENT OF SECOND EXPERIMENTAL MOTOR

	Predicted	FEA	Measured	Error (%)
Airgap flux (Wb)	0.0188	0.0190	0.0194	2.1
Magnet Flux (Wb)	0.0213	0.0200	\	6.5
Flux leakage in bridge (Wb)	0.0019	0.0023	\	17.4
Flux density bridge I (T)	2.51	2.45	\	2.4
Flux density in bridge II (T)	2.43	2.30	\	5.6

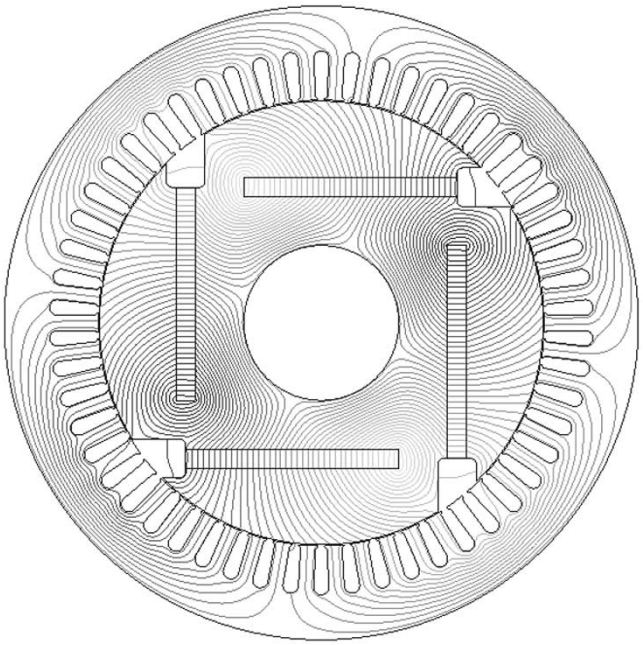

Fig. 14. Flux distribution of an asymmetrical-type, four-pole brushless IPM motor. The calculated air-gap flux is 0.0167 Wb by FEA and 0.0156 Wb by the proposed method, with the error being 7%.

For the first experimental motor, when the end effect is neglected, $\sigma_o = 1.337$. Further analysis of this coefficient reveals that the leakage coefficient is mainly related to the leakage flux in the magnetic bridge. For the first experimental motor, the leakage flux in the bridges accounts for 20% while the leakage in the rotor slot accounts for only 5% of total air-gap flux.

In order to understand the influence of magnetic bridge on air-gap flux and flux leakage, the size of the magnetic bridge of the first experimental motor was varied and the fluxes for each width and length are tabulated in Figs. 15 and 16.

It can be seen from Fig. 15 that when the width (cross-sectional area) of the magnetic bridge is fixed, the air-gap flux in-

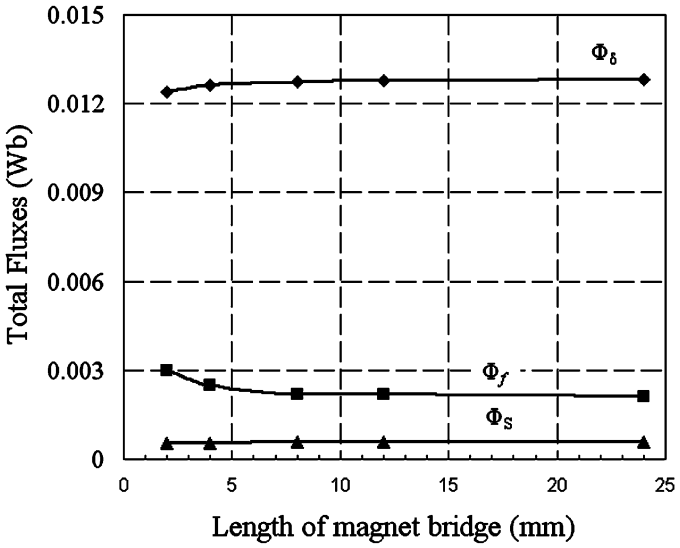

Fig. 15. Influences of the length of the magnetic bridges, with total bridge width of 5.2 mm.

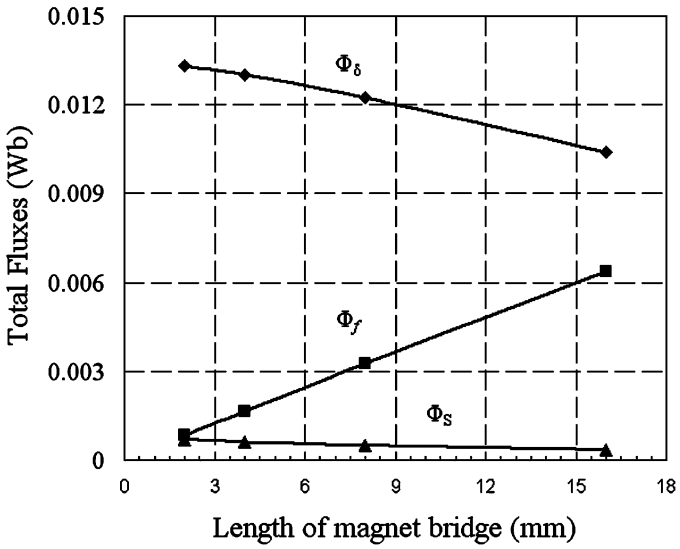

Fig. 16. Influences of the width of the magnetic bridges, with bridge length of 12 mm.

creases when the length of the magnetic bridge is increased. Magnetic flux in the bridge decreases with the increase of the length of the magnetic bridge. When the length of the bridge is larger than 10 mm, all fluxes reach a constant value.

It can be seen from Fig. 16 that when the length of the magnetic bridge is fixed, the air-gap flux decreases sharply with the increase of the cross-sectional area of the magnetic bridge, while the total flux in the bridge increases linearly due to a relatively constant flux density in the bridges.

Therefore, when designing an IPM motor, one should increase the length of the magnetic bridge while minimizing the cross-sectional area of the bridges. However, sufficient strength has to be kept for the rotor to withstand worst operation conditions of the motor.

X. Conclusion

This paper has proposed an analytical method to predict air-gap flux of IPM motors taking into account saturation, assembly gap, and flux leakage in the magnetic bridges. Detailed graphic analysis methods are provided with a simple Visual Basic program for Microsoft Excel. The method was validated through FEA analysis, and experimental measurements have also been made to add confidence to the results.

This simple analytical model for air-gap prediction should be of distinct values in design optimization studies where the large number of dimensional iterations precludes the use of finite-element analysis for PM motor design.

The method was illustrated with examples of both circumferential-type and radial-type IPM motors, verified by both line-start and brushless IPM motors. Therefore, it can be directly applied to all types of IPM designs. The method can also be applied to other types of PM motors, including brushless or synchronous PM motors with surface-mounted and inset magnets, by setting the width of the magnetic bridge to zero.

Acknowledgment

The authors would like to thank Dr. T. Sebastian of Delphi Automotive Systems for his valuable recommendations.

References

[1] M. N. Uddin, T. S. Radwan, and M. A. Rahman, "Performance of interior permanent magnet motor drive over wide speed range," *IEEE Trans. Energy Conversion*, vol. 17, pp. 79–84, Mar. 2002.

[2] J. F. Gieras and M. Wing, *Permanent Magnet Motor Technology: Design and Applications*, 2nd ed. New York: Marcel Dekker, 2002.

[3] G. R. Slemon and X. Liu, "Modeling and design optimization of permanent magnet motors," *Elect. Mach. Power Syst.*, vol. 20, pp. 71–92, 1992.

[4] T. J. E. Miller, *Brushless Permanent-Magnet and Reluctance Motor Drives*. Oxford, U.K: Clarendon, 1989.

[5] T. Kenjo and S. Nagamori, *Permanent Magnet and Brushless DC Motors*. Oxford, U.K.: Clarendon, 1985.

[6] V. B. Honsinger, "The field and parameters of interior type AC permanent magnet machines," *IEEE Trans. Power App. Syst.*, vol. 101, pp. 867–875, Apr. 1982.

[7] T. M. Jahns, G. B. Kliman, and T. W. Neumann, "Interior permanent magnet synchronous motors for adjustable-speed drives," *IEEE Trans. Ind. Applicat.*, vol. 22, pp. 738–747, July/Aug. 1986.

[8] Z. Q. Zhu, H. David, and C. C. Chan, "Improved analytical model for predicting the magnetic field distribution in brushless permanent-magnet machines," *IEEE Trans. Magn.*, vol. 38, pp. 229–238, Jan. 2002.

[9] M. A. Rahaman and G. R. Slemon, "Analytical models for interior-type permanent magnet synchronous motors," *IEEE Trans. Magn.*, vol. 21, pp. 1741–1743, Sept. 1985.

[10] C. C. Hwang and Y. H. Cho, "Effects of leakage flux on magnetic fields of interior permanent magnet synchronous motors," *IEEE Trans. Magn.*, vol. 37, pp. 3021–3025, July 2001.

[11] W. B. Tsai and T. Y. Chang, "Analysis of flux leakage in a brushless permanent-magnet motor with embedded magnets," *IEEE Trans. Magn.*, vol. 35, pp. 543–547, Jan. 1999.

[12] E. C. Lovelace, T. M. Jahns, and J. H. Lang, "A saturating lumped-parameter model for an interior PM synchronous machine," *IEEE Trans. Ind. Applicat.*, vol. 38, pp. 645–650, May–June 2002.

[13] S. Chen, *Electrical Machine Design* (in Chinese). Beijing, China: Mechanical Press, 1993.

[14] J. F. Chen, *Permanent Magnet Motors* (in Chinese). Beijing, China: Mechanical Press, 1983.

Chunting Mi (S'00–A'01–M'01–SM'03) received the B.S.E.E. and M.S.E.E. degrees from Northwestern Polytechnical University, Xi'an, China, and the Ph.D. degree from the University of Toronto, Toronto, ON, Canada, all in electrical engineering.

He is an Assistant Professor at the University of Michigan, Dearborn, with teaching responsibilities in the area of power electronics, electric vehicles, electric machines and drives. From 2000 to 2001, he was an Electrical Engineer with General Electric Canada Inc. He was responsible for designing and developing large electric motors and generators up to 30 MW. He started his career at the Rare-Earth Permanent Magnet Machine Institute of Northwestern Polytechnical University. He joined Xi'an Petroleum Institute as an Associate Professor and Associate Chair of the Department of Automation in 1994. He was a Visiting Scientist at the University of Toronto from 1996 to 1997. He has recently developed a Power Electronics and Electrical Drives Laboratory at the University of Michigan, Dearborn. His research interests are electric drives and power electronics, induction, brushless dc, and PM synchronous machines; renewable energy systems; electrical and hybrid vehicle power train design and modeling.

Dr. Mi is the Chair of the Power and Industrial Electronics Chapter of the IEEE Southeast Michigan Section.

Mariano Filippa (S'03) received the B.S.M.E. degree from the Technological Institute of Buenos Aires (ITBA), Buenos Aires, Argentina. He is pursuing the M.S. degree in automotive engineering at the University of Michigan, Dearborn.

He is currently a Research Assistant at the University of Michigan, Dearborn, working at the DTE Power Electronics Laboratory. He is responsible for the design of power electronic converters and testing equipment for motor control applications and laboratory testing. From 2001 to 2002, he was an Application Engineer at Asea Brown Boveri, Buenos Aires, Argentina, in the area of robotics. He had a key role in the engineering and construction of a fully automated robotized palletizing cell for the consumer industry. During 2002, he was also involved in research and development at the Technological Institute of Buenos Aires, designing a distributorless ignition system for laboratory research. His research interests are low and medium power electronics applications, ranging from control algorithms, EMI reduction and equipment design and testing, in the areas of motor control and hybrid vehicle applications.

Mr. Filippa has been a student member of ASME since 2000.

Weiguo Liu received the B.S.E.E. degree from Huazhong Polytechnical University, Wuhan, China, and the M.S.E.E. and Ph.D. degrees from Northwestern Polytechnical University, Xi'an, China.

He is Professor and Associate Chair of the Department of Automatic Control, Northwestern Polytechnical University. He joined Northwestern Polytechnical University in 1988 and has been performing research in rare-earth permanent-magnet machines and controls. His research interests are brushless dc machines, PM synchronous machines, dc machines, and induction machines.

Ruiqing Ma received the B.S.E.E., M.S.E.E., and Ph.D. degrees from Northwestern Polytechnical University, Xi'an, China.

He is Professor and Chair of the Department of Electrical Engineering, Northwestern Polytechnical University. He was with the Aerospace Research Institute from 1988 to 1996. He joined the Rare-Earth Permanent Magnet Research Institute in 1996. His research interests are vector control of PM and induction machines.